ROYAL SOCIETY
OF **CHEMISTRY**

PAPER
Linhao Hou *et al.*
Bioactive additives from the dorsal dermis of mice for
enhanced vascularization in 3D bioprinting

European
Society for
Biomaterials

Check for updates

Bioactive additives from the dorsal dermis of mice for enhanced vascularization in 3D bioprinting†

Yu Feng,‡[a,b] Linhao Hou,‡[a,c] Chao Zhang,‡[a,d] Liting Liang,[a] Qinghua Liu,[a] Zhao Li,[a] Wei Song,[a] Yi Kong,[a] Yaxin Tan,[a] Yuyan Huang,[a] Xu Guo,[a,e] Mengde Zhang,[a] Yuzhen Wang,[a] Jinpeng Du[a] and Sha Huang [ID] *[a]

Effective angiogenesis is essential for creating complex vascular networks in tissue engineering; however, there is a scarcity of safe and potent pro-angiogenic factors. Although a decellularized extracellular matrix (dECM) offers excellent biocompatibility and is widely used in tissue engineering as a pro-angiogenic additive, its conventional extraction technique resulting in significant loss of bioactivity limits clinical potential. The dorsal dermal tissue has rich blood perfusion and its dECM is rich in angiogenic factors. In this study, the dECM components from the dorsal dermis of mice (DD) were produced to enhance *in vitro* and *in vivo* pro-angiogenic abilities using a novel physical method. Morphological studies showed no significant difference between DD-wild-type (DD-wt) and DD-wild-type-newborn (DD-wtn), and there was also no difference in DNA or RNA concentration. In addition, DD-wtn outperformed DD-wt in maintaining the stemness of MSCs, promoting inflammatory response and facilitating endothelial cell differentiation. It is of greater significance to note that the dermal combined fibrous capsule thickness is greater in the DD-wt treated group than in the DD-wtn group. Furthermore, the number of blood vessels in the subcutaneously implanted scaffold with DD-wtn increased by 233%. Consequently, our current finding provides a promising strategy to produce a novel pro-angiogenic bioink additive for enhancing vascularization in 3D bioprinting.

1. Introduction

Vascularization is a crucial challenge in tissue engineering, particularly for creating larger tissues that can be properly perfused with nutrients and oxygen.[1–3] Several bioprinting materials have been developed to promote angiogenesis, such as tissue adhesives[4] and natural and synthetic materials laden with growth factors,[5–7] each exhibiting unique advantages and properties.[8] Poldervaart *et al.* reported a strategy that combined the controlled release of vascular endothelial growth factor (VEGF) from gelatin microparticles (GMPs) with Matrigel to sustain VEGF activity at desired locations within 3D bioprinted scaffolds. The release of VEGF from GMPs was confirmed for up to 3 weeks, which promoted the migration of human endothelial progenitor cells (EPCs) *in vitro* and improved vascularization *in vivo* in comparison to the rapid release group or control group. Additionally, compared to Matrigel alone, the application of this strategy resulted in improvements in gelation time, cell adhesion, and degradation speed. By utilizing these cutting-edge materials in bioprinting, vascular networks and blood vessels could be engineered, enabling the creation of functional and viable tissues for numerous biomedical applications.[9]

One promising approach for addressing the challenge of vascularization in tissue engineering is the use of bioinks that contain the decellularized extracellular matrix (dECM) with angiogenic properties, which can be incorporated into biprintable formulations.[10] This method allows for preserving the structural components and skeleton of the ECM while eliminating cellular components.[11] However, current methods for producing dECM mostly involve physical techniques such as repeated freeze–thaw cycles or sonication in combination with chemical agents or enzymes, resulting in the loss of most of the bioactive protein content.[12–14] As a result, alternative methods are required to preserve the abundant bioactive molecules in native tissues to produce angiogenic dECM for use in

[a]Research Center for Tissue Repair and Regeneration affiliated to the Medical Innovation Research Department, Chinese PLA General Hospital, 28 Fu Xing Road, Beijing, 100853, P. R. China. E-mail: stellarahuang@sina.com
[b]Department of Biomaterial, College of Life Sciences, Mudanjiang Medical University, Mudanjiang, 157011, China
[c]Cheeloo College of Medicine, Shandong University, Jinan, Shandong, 250012, PR China
[d]School of Medicine, Nankai University, 94 Wei Jing Road, Tianjin, 300071, PR China
[e]College of Graduate, Tianjin Medical University, 22 Qi Xiang Tai Road, Heping District, Tianjin, 300070, P.R. China
†Electronic supplementary information (ESI) available. See DOI: https://doi.org/10.1039/d4bm00957f
‡These authors contributed equally to this work.

bioinks. By addressing this issue, new approaches can be developed to create larger and well-perfused tissues with increased function and applicability for diverse biomedical purposes.

The dorsal dermis of mice provides an optimal environment for the growth and development of blood vessels. This region is also home to vital cells that regulate temperature, facilitate wound healing and tissue repair, and produce angiogenic factors.[15] Therefore, the dorsal dermis of mice has the potential to serve as a source of angiogenic factors for tissue engineering applications. However, further research is necessary to establish the suitability of dorsal skin for producing angiogenic bioinks.

Here, we propose a novel approach that extracts bioactive dECM components from the dorsal dermis of mice (DD) to strengthen the ability of vascularization as a new bioink additive. Firstly, we confirmed that this approach could remove cellular components, while retaining functional proteins. Also, dorsal dermis from adult and neonatal rats was selected to prepare the functional DD. Subsequently, we tested the physical properties of bioink containing DD. We continued to assess the impact of the DD additive on vascularization *in vitro* and *in vivo* (graphical abstract). The resulting bioinks can then be mixed with cells and other components to create complex structures that support widespread vascularization. Our current work offers a promising strategy for establishing extensive microvascular networks essential for tissue regeneration.

2. Materials and methods

All animal procedures were performed in accordance with the Guidelines for Care and Use of Laboratory Animals of the Chinese PLA General Hospital and approved by the Animal Ethics Committee of the Chinese PLA General Hospital (S2020-407-01).

2.1. Preparation of DD

Wild-type C57BL/6 mice were ordered from SPF Biotech (Beijing, China). Wild-type C57BL/6 neonatal mice were obtained from a normal laboratory breeding colony. The age and sex of the mice were controlled and maintained at consistent levels throughout the experiment. Briefly, we sacrificed the neonatal and 8-week-old mice. They were then immersed in 75% ethanol for 10 minutes. The mice were then rinsed twice with PBS. The dorsal skin of mice was excised with ophthalmic scissors and immersed in Red Blood Cell Lysis Buffer (Solarbio, China) for 10 minutes. After immersion, the dorsal skin was washed with PBS to remove residual liquid and then ground in a tissue homogenizer for 20 minutes. The entire grinding process was performed on ice. The supernatant was obtained after centrifugation at 10 000g for 20 min at 4 °C. Finally, the supernatant was filtered through a 0.22 μm filter, allowing for the successful preparation of DD-wild-type (DD-wt) and DD-wild-type-newborn (DD-wtn). The DD samples were stored at −80 °C until use.

2.2. Protein and nucleic acid concentration of DD

The protein concentration of DDs was determined using a BCA protein concentration assay kit (Solarbio, China). To calculate the total volume of the working solution based on the number of samples, the solutions of dioctylbutyric acid and copper ions were added to centrifuge tubes in a ratio of 50 : 1. They were mixed thoroughly. Then, 20 μl of 4 mg ml⁻¹ bovine serum albumin (BSA) sample was taken and mixed with 20 μl of dilution solution, phosphate-buffered saline (PBS), resulting in a concentration of 2000 μg ml⁻¹. From this mixture, 20 μl was taken and serially diluted. We obtained BSA standard solutions of concentrations 2000 μg ml⁻¹, 1000 μg ml⁻¹, 500 μg ml⁻¹, 250 μg ml⁻¹, 125 μg ml⁻¹, 62.5 μg ml⁻¹, 31.25 μg ml⁻¹, and 0 μg ml⁻¹, each with a volume of 20 μl. These solutions were added to the wells designated for protein standards in a 96-well plate. The samples were added to the sample wells in volumes of 0.5 μl, 1.0 μl, 2.0 μl, 4.0 μl, and 20.0 μl, followed by the addition of PBS to bring the total volume to 20 μl. Each concentration was replicated in three wells, and 20 μl of the dioctylbutyric acid working solution was added to each well. The plate was then incubated at 37 °C for 30 minutes. The absorbance values at 562 nm wavelength were measured using a multifunctional microplate reader to generate a standard curve. The protein concentrations of DD-wt and DD-wtn were calculated based on the standard curve. The experiment was repeated three times, and the data from the most representative set of results were selected. The protein concentrations of DD-wt and DD-wtn were diluted with PBS to be the same.

According to the protein concentration measured above, 50 μl of DD-wt and DD-wtn were diluted to the same concentration of 100 μg ml⁻¹. Then, 50 μl of the aforementioned DD-wt and DD-wtn were taken and placed onto a glass slide. After air-drying in a sterile ventilated hood, DAPI Fluoromount-G (0100-20, Southern Biotech) staining solution was added and allowed to act for 15 minutes. The samples were then observed under an inverted fluorescence microscope to assess the presence or absence of blue fluorescence, indicating the presence or absence of nuclear material in the DDs. Additionally, 10 μl of the aforementioned DD samples were taken for RNA and DNA quantification using a nanophotometer (Implen, Germany).

2.3. Cell isolation and culture

The isolation and culture protocols for mouse bone marrow mesenchymal stem cells (MSCs) were based on previous studies in our laboratory.[16,17] We purchased neonatal wild-type C57BL/6 mice from SPF Biotechnology (Beijing, China). Briefly, we sacrificed newborn mice and immersed them in 75% ethanol for 10 min, after which they were rinsed twice with PBS. The skin of the mice was removed from the dorsal portion using ophthalmic scissors. The muscles and soft tissues surrounding the femur and tibia were separated. The bilateral femur and tibia were placed into a sterile 100 mm Petri dish (Corning) containing complete MesenCult™ expansion medium (mice). The bones were crushed with hemostatic

forceps to release the bone marrow. The medium containing bone marrow was filtered with a 70 μm cell filter (BD Falcon). The separated cells were placed into a 100 mm culture dish and cultured at 37 °C and 5% CO_2. After 48 hours, the culture medium was changed. When the fusion efficiency reached 80%, cell passage was performed. We used third generation MSCs in this study.

2.4. CCK8 experiment

To understand the effect of DDs on cell proliferation, we performed the assay with Cell Counting Kit-8 (CCK-8; Dojindo, Japan). MSCs were inoculated 96-well plates at a density of 2000 cells per well. After adding 100 μl of complete MesenCult™ expansion medium (mice) to each well, they were incubated at a constant temperature of 37 °C in a CO_2 incubator. After cell apposition, the original medium was discarded and rinsed 3 times with PBS. The cells were divided into the following groups: control group, 100 μg ml^{-1} DD-wt group, 200 μg ml^{-1} DD-wt group, 500 μg ml^{-1} DD-wt group, 1000 μg ml^{-1} DD-wt group, 100 μg ml^{-1} DD-wtn group, 200 μg ml^{-1} DD-wtn group, 500 μg ml^{-1} DD-wtn group and 1000 μg ml^{-1} DD-wtn group, a total of 9 groups with 5 wells in each group. The control group was cultured in normal stem cell medium, and the remaining groups were cultured in medium containing the corresponding final mass concentration of DDs. The cells in each group were cultured for 24 h, and then 10 μl of the CCK-8 solution was added to each well and cultured for 2 h. The absorbance value at 450 nm was measured using a multifunctional enzyme marker to indicate the cell proliferation viability. The experiment was repeated three times.

2.5. Cell migration assay

To determine the effect of DDs on the migration capacity of MSCs, we performed scratch experiments. At the bottom of the 6-well plate, 6 marker lines were drawn in parallel. The MSCs were inoculated into 6-well plates at a concentration of 2×10^5 cells per ml, 2 ml per well. The experiment was divided into the following groups: normal medium control group, 100 μg ml^{-1} DD-wt group, 500 μg ml^{-1} DD-wt group, 100 μg ml^{-1} DD-wtn group and 500 μg ml^{-1} DD-wtn group, a total of 5 groups with 3 wells in each group. When the cell fusion reached 90%, the original medium was discarded and 3 parallel vertical marks were made vertically in the culture wells using a specified 200 μl pipette tip. The cells were washed 3 times with PBS to remove cell debris and impurities to ensure complete detachment of the scratched cells. After the scratch experiments, MSC medium containing 2% fetal bovine serum was added to each well. The images were collected at 0 h (immediately) and 24 h after scratching under an inverted fluorescence microscope. Three fields of view were selected for each group. The relative areas were calculated using ImageJ 1. 8. 0 image analysis software (National Institutes of Health, USA). The area at 0 h after scratching was recorded as S_0, and the area at 24 h after scratching was recorded as S. The cell migration rate was calculated as cell migration rate = $(S_0 - S)/S_0 \times 100\%$. This experiment was repeated three times.

2.6. Proteomic analyses

To determine the differences in the protein composition of DD-wt and DD-wtn, we performed a proteomic analysis. The proteomics of DDs was detected by the LC-Bio Company. When the p-value was less than 0.05 and the multiplicity of difference was greater than 2, it was considered significant and worthy of further study.

2.7. Preparation of DD-wt bioink and DD-wtn bioink

At this juncture, three distinct groups of bioinks were prepared: a basic bioink (control group), a DD-wt bioink (DD-wt group), and a DD-wtn bioink (DD-wtn group). The basic bioink consists of 3% (w/v) gelatin (Sigma-Aldrich, USA) and 1% (w/v) sodium alginate (Sigma-Aldrich, USA). Gelatin and sodium alginate were immersed in phosphate buffered saline (PBS) and heated at 70 °C to dissolve them. The dissolved alginate and gelatin (Alg-Gel) hydrogels were first immersed in a water bath at 70 °C for 30 minutes and then cooled at 4 °C for 5 minutes. The process was repeated 3 times for sterilization. The sterilized hydrogel was stored at 4 °C until use. The bioink was preheated at 37 °C and mixed with 500 μg ml^{-1} DD-wt or 500 μg ml^{-1} DD-wtn under aseptic conditions. The prepared bioinks were named DD-wt bioink or DD-wtn bioink and used for subsequent experiments. Bioinks containing mouse MSCs were prepared as follows: MSCs were added to the above prepared bioink at a concentration of 1×10^6 ml^{-1} and cells were uniformly dispersed in the bioink.

2.8. 3D bioprinting

3D bioprinting has been the subject of considerable attention due to its capacity to facilitate precise control over the spatial distribution of cells and biomaterials.[18] The strategy of bioprinting is based on our previous study.[19] The 3D bioprinting process was performed using a specific bioprinting platform called the Regenovo 3D Bioprinter, which was manufactured in China. To control the temperature of the process, a liquid temperature controller is used. To start the process, 5 ml of bioink was carefully transferred into a syringe that had been pre-sterilized. The syringe was then cooled to −20 °C for 10 minutes. After cooling, the syringe was mounted on the print arm of the bioprinter, which was set to a temperature of 10 °C. The sterilized 35 mm Petri dishes (Corning, USA) were placed on a platform pre-cooled to 4 °C. The printing process then began to build a 3D structure with specific dimensions. The final structure was 20 mm in length, 2.4 mm thick, and 0.3 mm apart. Layer by layer, the bioprinter carefully deposited the bioink to build the desired structure. To further solidify and stabilize the 3D bioprinted structures, cross-linking was performed immediately after printing. This was achieved by immersing the constructs in a sterilized calcium chloride solution at a concentration of 2.5%. The constructs were left in this solution for 10 minutes at room temperature. After the cross-linking process, the bioprinted constructs were rinsed twice with deionized water to remove the calcium chloride solution. Finally, the constructs were placed in complete

MesenCult™ expansion medium (mice) for subsequent experiments. The medium was changed every 3 days.

2.9. Scanning electron microscopy

The Christ Alpha 2-4 LD freeze dryer was used to freeze the bioink overnight. Subsequently, it was submerged in liquid nitrogen for 60 seconds and then broken with a freezing blade. After that, an Edwards sputter coater was employed to cover a 20 nanometer layer of gold on the bioink, which was left to dry for analysis. In the end, the bioink was observed by means of a Hitachi S-4800 scanning electron microscope from Japan.

2.10. Rheological test of bioink

The rheological test of the bioink was conducted on a rheometer (TA-ARESG2, USA) equipped with concentric plate sensors. The viscosity of the biological ink was tested at shear rates ranging from 0.1–100 s^{-1} at a temperature of 10 °C. A dynamic frequency scan was performed at a strain of 1% and a temperature of 10 °C to measure the storage modulus and the loss modulus.

2.11. Degradation of bioink

The 3D bioprinted constructs were immersed in Dulbecco's modified Eagle's medium (DMEM; Hyclone) and cultured under 37 °C and 5% CO_2 conditions. The 3D bioprinted constructs were weighed every 24 hours using an electronic balance (Sartorius, Germany). Sterile absorbent paper was used to absorb the moisture content of the 3D bioprinted constructs before weighing.

$$\text{Degradation rate } (\%) = (W_0 - W_I)/W_0 \times 100\%$$

where, W_0 was the initial value of the 3D bioprinted construct. W_I was the weight of the 3D bioprinted constructs measured at different immersion times, e.g., W_7 represented the weight of the 3D bioprinted construct after 7 days of immersion.

2.12. Release of protein in 3D bioprinted constructs

The three-dimensional bioprinted constructs containing DD-wt and DD-wtn were immersed in ultrapure water and cultured under the conditions of 37 °C and 5% CO_2. After 2, 6, 8, 12, and 24 hours, 100 μl of the culture medium was collected, and an equal volume of ultrapure water was added back simultaneously. The protein concentration in the culture medium was determined using the BCA protein assay kit, following the same BCA detection method as described in section 2.1.

2.13. Cell viability analysis

To observe the cell viability in the bioprinted constructs, a Live/Dead assay kit (L3224, Invitrogen) was used to distinguish live cells (green fluorescence) from dead cells (red fluorescence) under a fluorescent microscope (Olympus BX51). First, the 3D printed structures were placed in 35 mm glass-bottom confocal dishes (Beyotime, China) after one day of incubation. 3D printed structures were washed twice with Dulbecco's phosphate-buffered saline (DPBS) to remove residual culture medium. 5 μl of Calcein-AM solution and 20 μl of PI solution were added to 10 ml of DPBS and mixed thoroughly. The prepared liquid was added to the Petri dishes with 3 ml per dish. After incubation at 37 °C for one hour, the liquid in the Petri dishes was discarded and the 3D printed structures were rinsed twice with DPBS. Finally, we photographed the 3D printed structures with a fluorescence microscope.

2.14. Immunofluorescence staining

The bioprinted constructs were immobilized in formaldehyde polymer for 20 minutes and then dissolved in lysis buffer for 10 minutes. The lysis buffer was then centrifuged at 1500 rpm for 10 minutes to obtain the desired MSCs. MSCs were resuspended in 100 μl of PBS. Finally, the MSC suspension was added dropwise on an adhesive glass slide and dried at room temperature for the following tests. The lysis buffer consisted of ethylenediamine tetraacetic acid disodium salt (EDTA, 0.05 M), sodium chloride (0.15 M) and sodium citrate (0.06 M).[20] After antigen retrieval, infiltration, and blocking, the slides were incubated with primary antibodies at 4 °C overnight and secondary antibodies at room temperature for 2 h. The primary antibodies used in these experiments were Anti-Ki67 antibody (1 : 250, ab16667, Abcam), Anti-CD31 antibody (1 : 300, 66065-2-Ig, Proteintech), Anti-Oct-4 antibody (1 : 300, ab18976, Abcam), Anti-TNF-α antibody (1 : 1000, ab66579, Abcam), Anti-TGF Beta 1 antibody (1 : 500, 21898-1-AP, Proteintech), Anti-IL-10 antibody (1 : 250, ab133575, Abcam), and Anti-IL-6 antibody (1 : 250, ab290735, Abcam). The secondary antibodies used in these experiments were CoraLite594-conjugated Goat Anti-Mouse IgG (H + L) (1 : 300, SA0013-3, Proteintech), CoraLite594-conjugated Goat Anti-Rabbit IgG (H + L) (1 : 300, SA00013-4, Proteintech), and CoraLite488-conjugated Goat Anti-Rabbit IgG (H + L) (1 : 300, SA00013-2, Proteintech). Finally, the nuclei were stained with DAPI Fluoromount-G (0100-20, SP8 FALCON, Germany).

2.15. Construction of a subcutaneous mouse implant model

To examine the effect of DDs on angiogenesis, we buried 3D printed structures under the skin of mice. The experiments were divided into three groups based on the type of ink, namely, Alg-Gel hydrogels (control group), Alg-Gel-DD-Wt hydrogels (DD-Wt group) and Alg-Gel-DD-Wtn hydrogels (DD-Wtn group). Three mice were used in each group. C57BL/6 mice (SPF Biotechnology Company, China) were anesthetized with pentobarbital (100 mg kg^{-1}) preoperatively. The mice were placed in a prone position. We shaved the dorsal hair of the mice and made a 20 mm incision in the dorsal midline. The cell-laden bioprinted constructs were grafted subcutaneously. The incision was sutured after grafting. The mice in each group were sacrificed, and bioprinted constructs with skin were sampled on day 3, day 7, and day 14. The extracted tissues were fixed with 40 g L^{-1} paraformaldehyde, which ensured their preservation and readiness for further experiments.

2.16. Histological and immunofluorescence analysis

The tissues were paraffin-embedded and sectioned (5 μm thicknesses). Sections were stained with hematoxylin and eosin

(H&E) according to conventional histological methods. After the sections were dewaxed and rehydrated using xylene and gradient ethanol, they underwent staining with hematoxylin for 10 minutes and eosin for 1 minute. Following staining, the tissues were carefully sealed with neutral resin to protect them and facilitate long-term preservation. The sealed tissues were then observed under a microscope (ECHO Revolve, American).

Immunofluorescence staining of sections also needs dewaxing and rehydration using xylene and gradient ethanol. The remaining operation was the same as in section 2.14. The primary antibodies used in these experiments were anti-CD31 antibody (1 : 200, ab284583, Abcam) and anti-α-SMA antibody (1 : 500, ab7817, Abcam). The secondary antibodies used in these experiments were CoraLite488-conjugated Goat Anti-Mouse IgG (H + L) (1 : 300, SA0013-3, Proteintech) and CoraLite594-conjugated Goat Anti-Rabbit IgG (H + L) (1 : 300, SA00013-4, Proteintech).

2.17. Statistical analyses

All data were expressed as the means ± SD. All data were analyzed by one-way ANOVA or Student's t-test. Statistical significance was determined with p-values <0.05.

3. Results

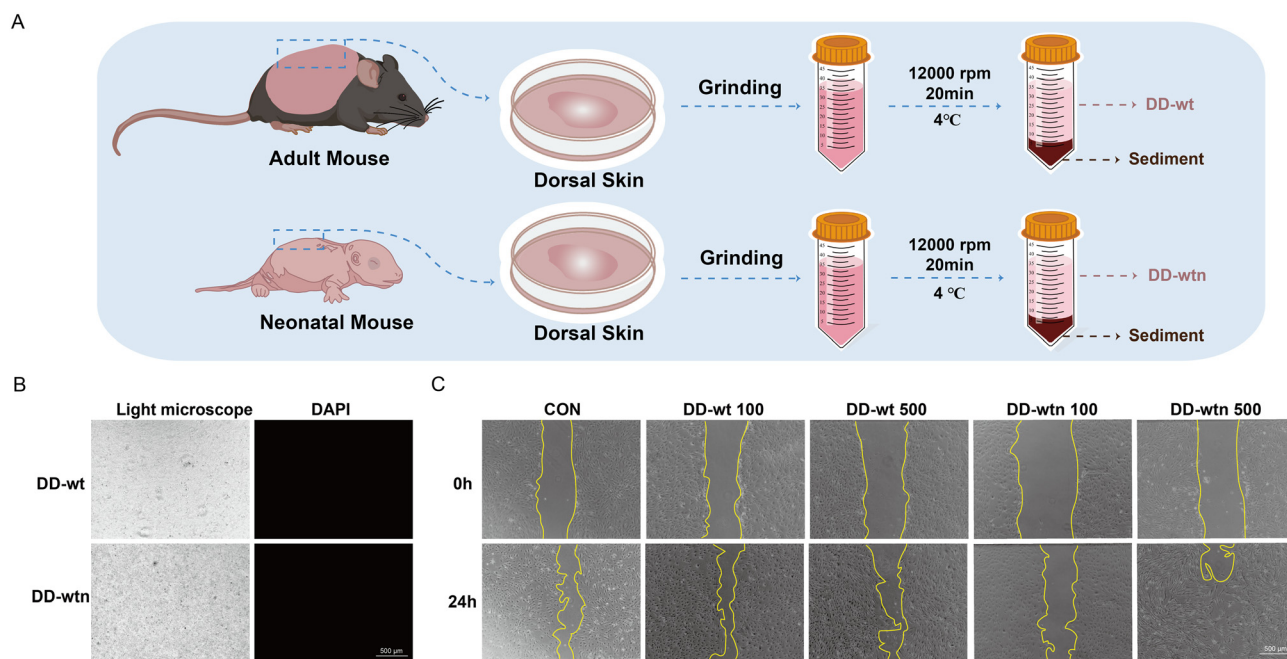### 3.1. DD promotes cell aggregation and proliferation

The procedure for preparing DD is shown schematically in Fig. 1A. When DD-wt and DD-wtn were observed under a light microscope, the morphology of the two was not significantly different (Fig. 1B). Measurement of protein concentration, DNA concentration, and RNA concentration of DD revealed that the protein concentration of extracted DD-wt was three times higher than that of DD-wtn (Fig. S1A†), and there was no significant difference in DNA concentration and RNA concentration (Fig. S1B and C†). The stained nuclei were not visible when we detected immunofluorescence after labeling DD-wt and DD-wtn with DAPI (Fig. 1B).
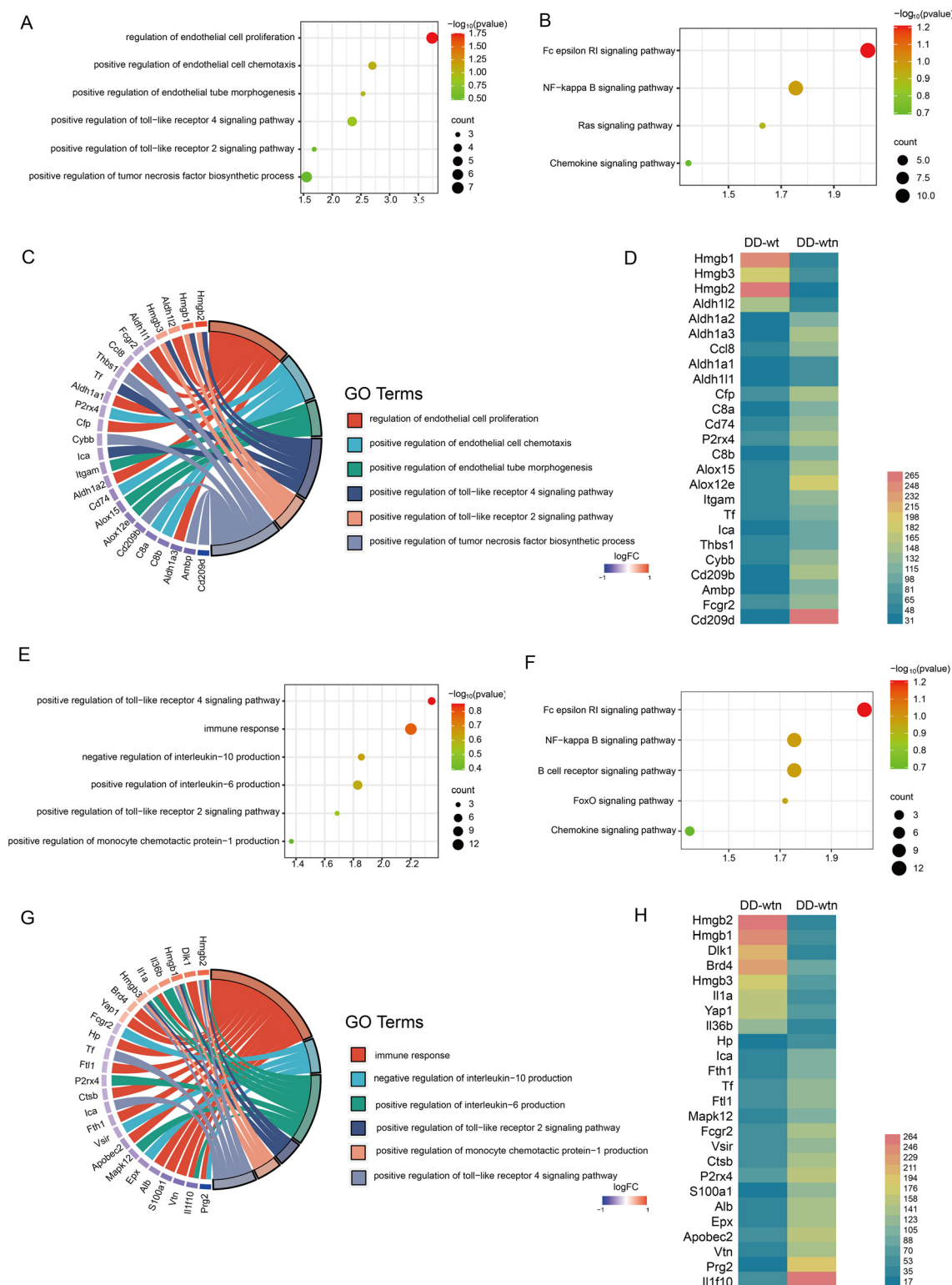
We conducted CCK8 and scratch experiments to investigate the impact of extracted DD on the state of MSCs. Among the four concentration gradients (100, 200, 500, 1000 μg ml^{-1}) and eight groups (four groups of DD-wt and four groups of DD-wtn), only 1000 μg ml^{-1} of DD-wt and 1000 μg ml^{-1} of DD-wtn would inhibit the proliferation of stem cells (Fig. S1D†). 500 μg ml^{-1} of DD-wtn had a significant effect on the migration of mesenchymal stem cells within 24 hours, as demonstrated by the DD scratch experiment results (Fig. 1C and S1E†).

3.2. DD-wt and DD-wtn have distinct protein expressions

We screened and quantified proteins expressed by DD-wt and DD-wtn using quantitative proteomics analysis to explore the possible mechanisms of action of age factors affecting DD. According to the quantitative proteomics results, DD-wt and DD-wtn had hardly any differences in protein composition, but there were significant differences in the concentration levels of certain proteins. Angiogenic and inflammatory pathways had higher concentrations of different proteins, as determined by Gene Ontology (GO) analysis and Kyoto Encyclopedia of Genes and Genomes (KEGG) analysis (Fig. 2A, B, E and F).

Fig. 1 Schematic illustration of the extraction and preparation process of bioactive ECM components from the dorsal dermis of mice (DD) and its effect on the migration of mesenchymal stem cells (MSCs). (A) Schematic description. (B) Representative microscopic and fluorescent images of DD (scale bar, 500 μm). (C) Results of MSC migration at 24 hours of culture (scale bar, 500 μm).

Fig. 2 Proteomic analysis of DD. (A) GO analysis related to angiogenesis. (B) KEGG analysis related to angiogenesis. (C) Correspondence between angiogenesis-related entries and genes in GO analysis. (D) Differential expression of angiogenesis-related genes. (E) GO analysis related to inflammation. (F) KEGG analysis related to inflammation. (G) Correspondence between inflammation-related entries and genes in GO analysis. (H) Differential expression of inflammation-related genes.

The first step in determining the GO analysis's correlation between angiogenesis-related entries and genes was to determine the correspondence. We screened for genes with high mobility group box 2 (Hmgb2) and high mobility group box 1 (Hmgb1) with a large multiplicity of differences, which correspond to the toll-like receptor pathway (Fig. 2C). To acquire additional information about the relevant differential genes, we conducted an expression profile analysis of angiogenic genes. It was found that Hmgb2 and Hmgb1 not only had significant differences in protein expression between DD-wtn and DD-wt, but also had a high expression status in DD-wtn according to the results (Fig. 2D).

We analyzed the relationship between inflammation-related entries and genes and conducted an analysis of their expression. Surprisingly, Hmgb2 and Hmgb1, which also play a role in inflammation, corresponded as the genes with the highest multiplicity of differences among the related entries to the toll-like receptor pathway, interleukin 10, and monocyte chemotactic protein-1 secretion (Fig. 2G). The expression of Hmgb2 and Hmgb1 was consistent with Fig. 2D, according to the differential expression of inflammation-producing genes (Fig. 2H).

3.3. The physical properties of bioinks remain unaffected by the addition of DD

We were interested in determining the physical properties of bioinks by adding DD-wt and DD-wtn. The morphology of gelatin in bioinks was monitored before and after adding DD to investigate its impact on its thermal cross-linking properties. We found that the transparency of the DD-wt and DD-wtn groups was slightly lower than that of the control group, but all three groups had good flowability and the same coagulation effect (Fig. 3A). We produced three different types of bioinks using 3D printing technology, and through a cross-linking process, we successfully converted them into solid structures. Upon observing the final printed structures, we noticed that all three groups of structures retained their original shape and exhibited remarkable transparency, which proved their excellent printability (Fig. 3A). Scanning electron microscopy results showed that the addition of DD-wt and DD-wtn did not significantly change the pore size of the bioinks compared to the control group (Fig. 3B), remaining around 100–120 μm (Fig. 3C). Rheological tests showed that the viscosity of all groups decreased with increasing shear rate, and all three groups were able to form gels in a relatively short period of time (Fig. 3D and E). In addition, we tested the effect of DD on the degradation rate of the bioink. The results showed that the addition of DD also had no significant effect on the degradation of the bioink (Fig. 3F and G). Protein release results showed that both DD-wtn and DD-wt had a high release rate of about 80% in 24 hours. This implies that these two proteins have a high capacity to release their constituent molecules in a relatively short period of time (Fig. 3H). Finally, we also tested the effect of DD-added bioink on MSC survival. Cell live-dead staining results showed that the addition of DD had no effect on cell survival (Fig. 3I and J).

3.4. Effects of three-dimensional bioprinting microenvironment on the biological behavior of MSCs

After culturing the bioprinted structures in MesenCult™ Extended Medium for 1 day, the bioprinted bodies were lysed out of the cells for extensive analysis to assess the expression levels of different markers associated with the proliferation, stemness, and secretory capacity of MSCs in each group. The results showed that the expression of Oct-4, a stemness-related marker, was significantly higher in MSCs from the DD-wtn group compared to the control and DD-wt groups (Fig. 4A and C), and the expression of Ki67 was not significantly different between the groups (Fig. 4B and D).
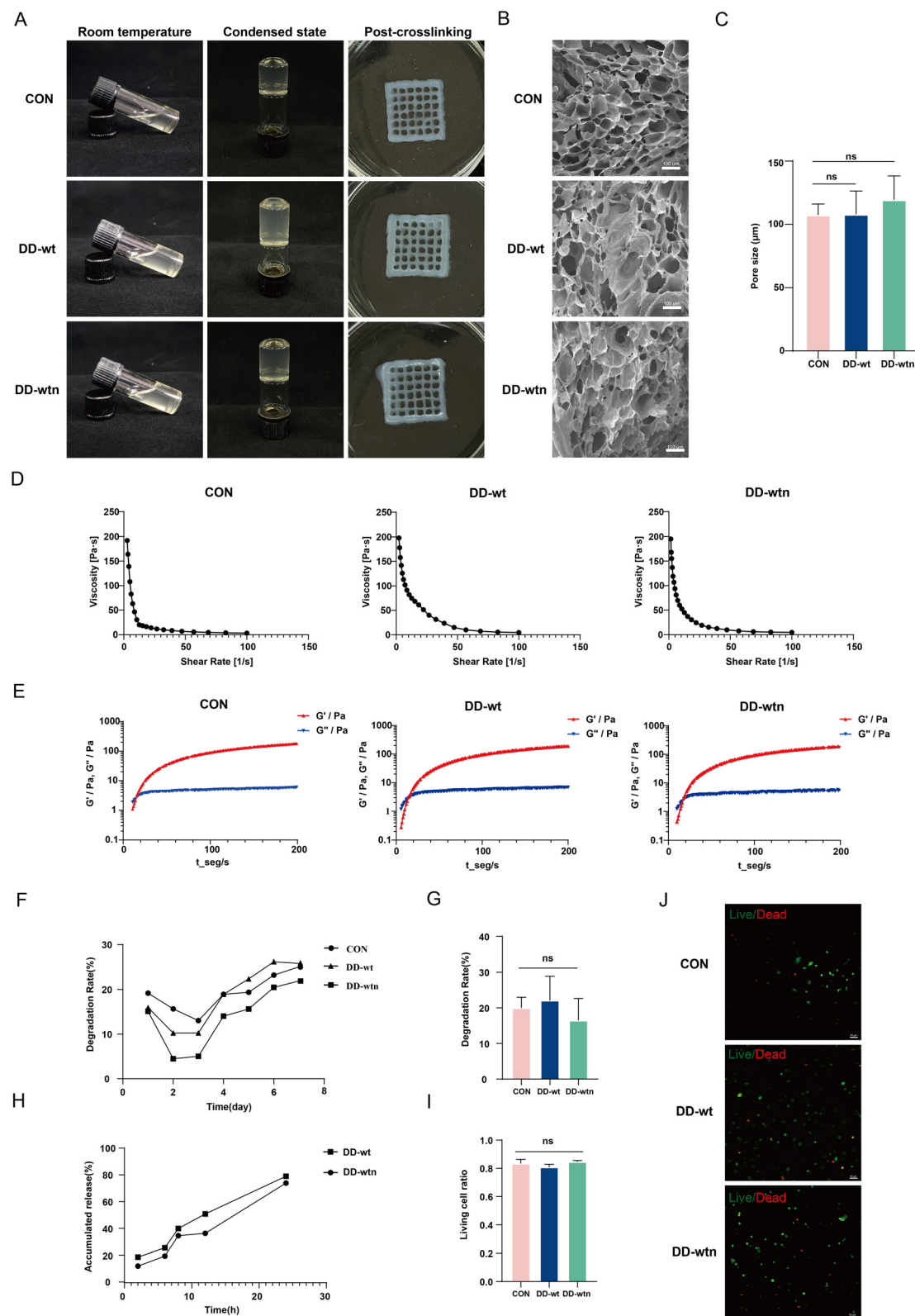
In terms of cytokine secretion, the expression of IL-6 was significantly higher in MSCs from both DD-wtn and DD-wt groups compared with the control group (Fig. 4E and G). The expression of IL-10 in the DD-wtn group was significantly lower than that in the control and DD-wt groups (Fig. 4F and H). Compared with the control group, the expression of TGF-β1 was significantly higher in both the DD-wtn and DD-wt groups (Fig. 4I and K). In addition, the expression levels of MSC differentiation markers were detected after 5 days of continuous culture in MesenCult™ Expansion Medium. The expression of the differentiation marker CD31 was significantly higher in MSCs from the DD-wtn group compared to the control and DD-wt groups (Fig. 4J and L). There were no significant differences in TNF-α and VEGF expression levels between DD-wtn and DD-wt (Fig. S1F, G, H and I†).
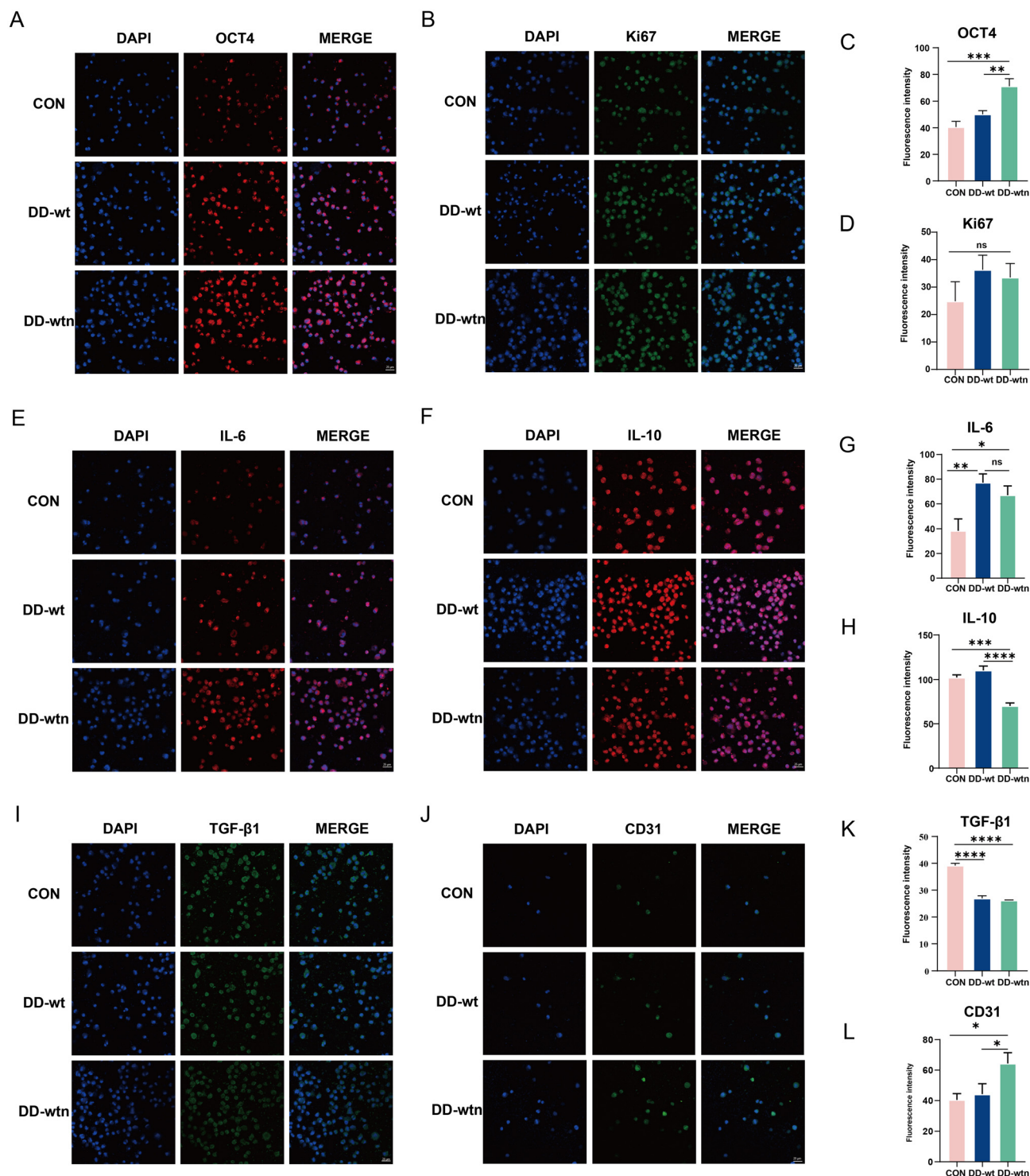
3.5. DD-wtn promotes angiogenesis

We verified the role of DD *in vivo* by implanting the model on the backs of mice. The construction of three groups of implants was achieved through the utilisation of three distinct groups of bioinks (Alg-Gel hydrogels, Alg-Gel-DD-Wt hydrogels and Alg-Gel-DD-Wtn hydrogels) as raw materials, in conjunction with the incorporation of MSCs as seeds. Subsequently, the implants were then implanted in the backs of the mice, as illustrated in Fig. 5a. According to our findings, the thickness of the capsule around the tissue gradually increased over time. It was surprising to see that the fibrous capsule in the DD-wtn group was significantly thicker than that in the control group after 7 days; capsule thickness did not differ significantly between the DD-wt and DD-wtn groups at this time. Nevertheless, when the experiment's duration was extended to 14 days, the DD-wtn-parts were observed to have a statistically significant rise in capsule thickness compared to the control and DD-wt-parts (Fig. 5B and C). Next, we assessed the vascularization within the 3D printed tissues and found a significant increase in vascularization within the printed tissues as well as in the surrounding fibrous capsule in the DD-wtn-group compared to the DD-wt-group and the control group. This discovery demonstrates the potent ability of the substances in the DD-wtn group to promote angiogenesis (Fig. 5D and E).

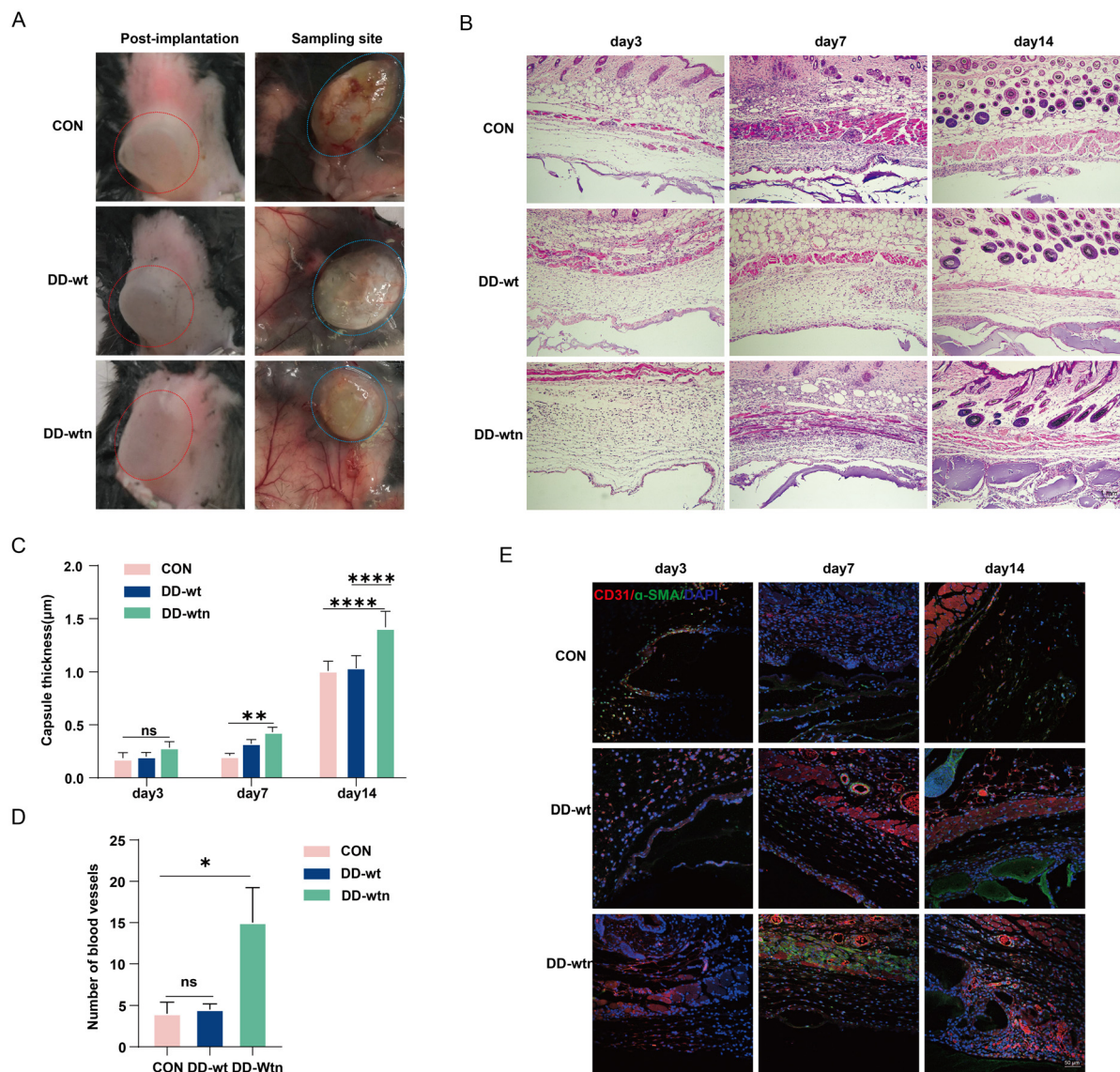Our findings indicate that neonatal mouse-derived DD significantly promotes the vascularization of 3D printed con-

Fig. 3 The addition of DD does not affect the physical properties of bioink. (A) Observation of the contraction and crosslinking of normal bioink and bioink with DD-wt and DD-wtn at room temperature. (B) SEM microstructure (scale bar: 100 μm). (C) Pore size statistics of bioink. (D) Performance testing of shear deformation of bioink. (E) Gelation time detection of bioink. (F) Degradation curve of bioink. (G) Degradation rate of bioink-containing cell constructs. (H) Protein release rate in bioink. (I) Ratio of live cells in bio-printed constructs. (J) Viability staining of MSCs in bio-printed constructs (scale bar: 50 μm). ns: $p > 0.05$, *$p < 0.05$.

Fig. 4 Biological behavior of MSCs in 3D bioprinted constructs. (A, B, E, F and I) Immunofluorescence imaging of Oct-4, Ki67, IL-6, IL-10 and TGF-β1 in bioprinted constructs after being cultured for 1 day *in vitro* (scale bar: 25 μm). (J) Immunofluorescence imaging of CD31 in bioprinted constructs after being cultured for 5 days *in vitro* (C, D, G, H, K and L) quantitative analysis of Oct-4, Ki67, IL-6, IL-10, TGF-β1 and CD31 fluorescence. ns: $p > 0.05$, *$p < 0.05$, **$p < 0.01$, ***$p < 0.001$, ****$p < 0.0001$.

Fig. 5 Angiogenesis of 3D bioprinted constructs *in vivo*. (A) Image of the placement of bioprinted constructs and the sampling site. (B) Images of H&E staining of bioprinted constructs buried under the skin (scale bar: 1 mm). (C) Thickness statistics of the fibrous capsule of the 3D printed structure. (D and E) Images of immunofluorescence staining of bioprinted constructs buried under the skin and quantitative analysis (scale bar: 50 μm). ns: $p > 0.05$, **$p < 0.01$, ****$p < 0.0001$.
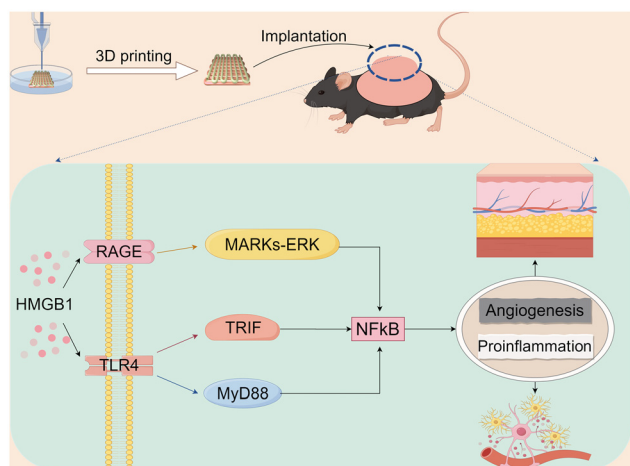
structs. In addition, as confirmed by GO and KEGG analyses, this may be related to the proinflammatory and angiogenic effects of HMGB1 (Fig. 6).

4. Discussion

The bioprinting materials that promote vascular regeneration have been widely used in various biomedical applications. Among these, the most promising is the use of dECM as an additive to enhance vascular regeneration.[21] However, due to the limitations of the extraction techniques for decellularized ECM, most of the bioactive components are difficult to preserve, leading to a limited demonstration of the advantages of

the biomaterials.[22–24] Therefore, there is an urgent need for a new method to retain the rich bioactive molecules from native tissues, amplify their vascular regenerative function, and facilitate a new advancement in their biomedical applications. The dermis of mice is rich in blood vessels and lymphatics, which provide abundant oxygen and nutrients, regulate skin surface temperature, and serve as conduits for immune cell transport.[25] Experiments have shown that dermal fibroblasts secrete pro-angiogenic factors that can penetrate the collagen matrix and stimulate vascular assembly.[26] Additionally, preliminary studies by our research group have found that the number of blood vessels in the dermis of neonatal mice far exceeds that of adult mice, indicating that the dermis of neonatal mice might be a novel source of angiogenic factors for

Fig. 6 DD-wtn promotes pro-inflammation and angiogenesis through the Hmgb1-mediated NF-κB pathway (diagram by FigDraw).

biomedical applications.[27] Therefore, in this study, we avoided traditional ECM extraction methods and developed a new method for extracting bioactive ECM components with maximum preservation of bioactivity from the dermis of mice (DD).

This procedure demonstrated that our extraction method is efficient and feasible. In terms of morphology and biocompatibility, DDs extracted from neonatal and adult mice showed consistency, suggesting that the structure and function of DDs remain stable during development. In addition, the results of immunofluorescence staining further confirmed the purity of the DD samples, and the absence of cellular nuclear labeling was shown to imply that the DD samples did not contain cellular components, which is crucial for subsequent biomedical applications as it ensures that the DDs do not elicit an immune response when applied *in vivo*. Our results also indicate that DD, as an aggregate of bioactive components, has a significant effect on the behavior of mesenchymal stem cells (MSCs). High concentrations of DD-wt and DD-wtn (1000 μg ml^{-1}) exhibited inhibitory effects on the proliferation of MSCs, which may be due to the possible toxic effects of high concentrations of the bioactive substances on the cells or due to the changes in the intracellular signaling pathways at high concentrations. In contrast, 500 μg ml^{-1} of DD-wtn significantly promoted the migration of MSCs, a finding that suggests DD-wtn may contain specific factors that promote cell migration and these factors are able to activate cell migration-related signaling pathways at appropriate concentrations. The results of the cell proliferation and migration assays emphasized the importance of DD concentration and also revealed age as a key factor influencing the effectiveness of DD. This finding provides important insights into the need to consider age-related changes when conducting DD-related research and applications, and to optimize the concentration of DD to obtain the best results.

Proteomics is the study of the proteome, and identifying differentially expressed proteins between treatment groups is an important goal of proteomics research.[28] Our proteomics analyses revealed significant differences between DD in neonatal and adult mice, and the identification of these differentially expressed proteins provides a molecular basis for understanding the differential effects of DD on cell behavior. Through GO enrichment and KEGG pathway analysis, we found that these differentially expressed proteins were mainly associated with angiogenesis and inflammatory responses, suggesting that DD may influence cell fate by regulating these biological processes. Of particular note, we identified a number of proteins associated with positive regulation of endothelial cell proliferation and chemotaxis, which may be related to the ability of DD to promote cell migration. In addition, proteins associated with the positive regulation of tumor necrosis factor biosynthetic processes may explain the potential role of DD in the inflammatory microenvironment. Our findings also highlight the importance of IL-10, IL-6, chemokine signaling pathways, and NF-κB signaling pathways in the mechanism of action of DD, which play key roles in the regulation of immune response and inflammatory response. These findings provide new insights into the application of DD in tissue repair and inflammation-related diseases.

HMGB2 and HMGB1 are important proteins in the high mobility group box protein family and have been extensively studied for their roles in inflammation and angiogenesis.[29–31] Our gene expression analysis showed that the protein expression of HMGB1 and HMGB2 was significantly higher in DD-wtn than in DD-wt. HMGB1, as a damage-associated molecular pattern (DAMP), plays a key role in the progression of inflammatory and angiogenic diseases.[32] Studies have shown that HMGB1 overexpression or administration has a significant impact on vessel density and recovery in skin wounds, ischemic hindlimbs, or myocardium,[33–35] whereas inhibition of HMGB1 could reverse its proinflammatory or proangiogenic effects.[35,36] Our findings suggest that the high expression of HMGB1 in DD-wtn may be associated with the positive role of DD-wtn in promoting cell migration and angiogenesis. In addition, overexpression of HMGB2 may also be involved in the biological activity of DD-wtn. Although the specific mechanism of HMGB2's role in angiogenesis and inflammation is not fully understood, our findings suggest that HMGB2 may act synergistically with HMGB1 to co-regulate these biological processes.

Our results show that the introduction of DD does not adversely affect the key physical properties of bioinks, such as viscosity, porosity and printing speed. This finding provides an important practical basis for the application of DD as a novel bioink additive. By comprehensively evaluating the bioink at room temperature and in the condensed state, we confirmed that the addition of DD does not affect its appearance, gel time, and printability, which further supports the potential application of DD in bioprinting. At the cellular level, we found that neonatal mouse DD had a significant effect on maintaining the stemness of mesenchymal stem cells (MSCs) and promoting their differentiation into endothelial cells, suggesting that DD may contain specific factors that regulate

cell fate. In addition, the regulatory effect of DD on the inflammatory microenvironment was an important finding, in which changes in the expression of IL-6 and IL-10 suggested that DD might have pro-inflammatory properties. Although the incorporation of DD did not have a significant effect on the proliferation of MSCs, it showed advantages in its ability to maintain cell stemness and promote differentiation, which is important for the fields of tissue engineering and regenerative medicine. Bioinks exhibit pore sizes suitable for cell survival and suitable degradation rates while maintaining good fluidity, gelling ability and transparency, properties that are essential for printing 3D cellular structures.

The results of the *in vivo* experiments further solidify our finding that the addition of DD in neonatal mice significantly promotes the vascularization of 3D printed constructs. This finding not only confirms the presence of angiogenesis-promoting factors in DD, but also suggests that these factors remain effective in the *in vivo* environment. This provides an important theoretical basis for the use of DD in tissue engineering and regenerative medicine, especially in applications that require the promotion of neovascularization, such as cardiovascular tissue engineering and wound healing models. Notably, the thickening of the fibrous capsule around the printed structures in the DD group of neonatal mice suggests that the addition of DD may have promoted an inflammatory response. This inflammatory response may be due to the activation of local immune cells by certain components of DD or to the fact that DD promotes the inflammatory response that accompanies the angiogenic process. Although the inflammatory response may promote tissue repair to some extent, excessive inflammation may also adversely affect the tissue-engineered structures. Therefore, more in-depth studies on DD-induced inflammatory responses are needed to optimize its application in bioinks. In addition, our findings emphasize the importance of the age factor in the role of DD. Neonatal mouse DD was significantly more effective than adult mouse DD in promoting angiogenesis, suggesting that the biological activity of DD may vary with age. This finding suggests that the age of the source mice needs to be considered when selecting DD as a bioink additive to ensure that optimal biological activity is obtained.

Our study not only provides a new theoretical basis for the application of DD-wtn in tissue repair and regeneration, but also provides new ideas for developing therapeutic strategies targeting HMGB1 and HMGB2. Future studies should further explore the mechanism of action of HMGB1 and HMGB2 in DD-wtn and how they affect cell behavior and therapeutic response. In addition, investigating the potential application of inhibitors or antagonists of HMGB1 and HMGB2 in regulating DD bioactivity may provide new therapeutic strategies for the treatment of inflammation- and angiogenesis-related diseases.

5. Conclusion

In this study, we developed a method for the first time to extract bioactive ECM components from the dorsal dermis of neonatal mice and focused on the effect of physical extraction methods on the maintenance of the active components of ECM proteins. Through proteomic analysis, we found that the dermis of neonatal mice was enriched with pro-angiogenic and pro-inflammatory genes, which were significantly different from the dermal composition of adult mice. Further *in vitro* experiments confirmed that DD-wnt derived from neonatal mice was effective in promoting angiogenesis and inflammatory responses in mesenchymal stem cells (MSCs). In *in vivo* experiments, we implanted three-dimensionally printed scaffolds containing DD-wnt and MSCs into a mouse model and observed significant inflammatory and angiogenesis-enhancing effects. These findings provide novel strategies for the development of pro-angiogenic bioinks, which are of great significance for addressing vascularization challenges in tissue engineering.

Author contributions

Yu Feng: collection of data, data analysis and interpretation, and manuscript writing. Linhao Hou: assembly of data and manuscript writing. Chao Zhang: conception and design, and assembly of data. Liting Liang, Qinghua Liu, Zhao Li, Wei Song, Yi Kong, Yaxin Tan, Yuyan Huang, Xu Guo, Mengde Zhang, Yuzhen Wang, and Jinpeng Du: administrative support and assembly of data. Sha Huang: conception and design, provision of study materials, final approval of manuscript, and financial support.

Data availability

The data that support the findings of this study are available from the corresponding author upon reasonable request.

Conflicts of interest

All authors declare that they have no financial or non-financial interests directly or indirectly related to the work submitted for publication.

Acknowledgements

References

1 J. Fu and D.-A. Wang, In Situ Organ-Specific Vascularization in Tissue Engineering, *Trends Biotechnol.*, 2018, **36**(8), 834–849, DOI: **10.1016/j.tibtech.2018.02.012**.

2 J. Rouwkema and A. Khademhosseini, Vascularization and Angiogenesis in Tissue Engineering: Beyond Creating Static Networks, *Trends Biotechnol.*, 2016, **34**(9), 733–745, DOI: **10.1016/j.tibtech.2016.03.002**.

3 Y. Zhao, M. Li, J. Mao, Y. Su, X. Huang, W. Xia, X. Leng and T. Zan, Immunomodulation of wound healing leading to efferocytosis, *Smart Med.*, 2024, **3**(1), e20230036, DOI: **10.1002/SMMD.20230036**.

4 B. Kong, C. Qi, H. Wang, T. Kong and Z. Liu, Tissue adhesives for wound closure, *Smart Med.*, 2023, **2**(1), e20220033, DOI: **10.1002/SMMD.20220033**, PMID: 39188560; PMCID: PMC11235766.

5 E. C. Novosel, *et al.*, Vascularization is the key challenge in tissue engineering, *Adv. Drug Delivery Rev.*, 2011, **63**(4–5), 300–311, DOI: **10.1016/j.addr.2011.03.004**.

6 J. Ma, *et al.*, 3D Printing of Strontium Silicate Microcylinder-Containing Multicellular Biomaterial Inks for Vascularized Skin Regeneration, *Adv. Healthcare Mater.*, 2021, **10**(16), e2100523, DOI: **10.1002/adhm.202100523**.

7 J. Bian, L. Bao, X. Gao, X. Wen, Q. Zhang, J. Huang, Z. Xiong, F. F. Hong, Z. Ge and W. Cui, Bacteria-engineered porous sponge for hemostasis and vascularization, *J. Nanobiotechnol.*, 2022, **20**(1), 47, DOI: **10.1186/s12951-022-01254-7**.

8 Y. Zhu, B. Kong, R. Liu and Y. Zhao, Developing biomedical engineering technologies for reproductive medicine, *Smart Med.*, 2022, **1**(1), e20220006, DOI: **10.1002/SMMD.20220006**, PMID: 39188735; PMCID: PMC11235786.

9 M. T. Poldervaart, *et al.*, Prolonged presence of VEGF promotes vascularization in 3D bioprinted scaffolds with defined architecture, *J. Controlled Release*, 2014, **184**, 58–66, DOI: **10.1016/j.jconrel.2014.04.007**.

10 A. C. Hielscher and S. Gerecht, Engineering approaches for investigating tumor angiogenesis: exploiting the role of the extracellular matrix, *Cancer Res.*, 2012, **72**(23), 6089–6096, DOI: **10.1158/0008-5472.CAN-12-2773**.

11 L. Leng, *et al.*, Comprehensive proteomic atlas of skin biomatrix scaffolds reveals a supportive microenvironment for epidermal development, *J. Tissue Eng.*, 2020, **11**, 2041731420972310, DOI: **10.1177/2041731420972310**.

12 S. P. Roth, *et al.*, Automated freeze-thaw cycles for decellularization of tendon tissue - a pilot study, *BMC Biotechnol.*, 2017, **17**(1), 13, DOI: **10.1186/s12896-017-0329-6**.

13 C.-H. Lin, *et al.*, Sonication-Assisted Method for Decellularization of Human Umbilical Artery for Small-Caliber Vascular Tissue Engineering, *Polymers*, 2021, **13**(11), 1699, DOI: **10.3390/polym13111699**.

14 S. Lee, *et al.*, Enhanced Regeneration of Vascularized Adipose Tissue with Dual 3D-Printed Elastic Polymer/dECM Hydrogel Complex, *Int. J. Mol. Sci.*, 2021, **22**(6), 2886, DOI: **10.3390/ijms22062886**.

15 J. Ohtola, *et al.*, beta-Catenin has sequential roles in the survival and specification of ventral dermis, *Development*, 2008, **135**(13), 2321–2329, DOI: **10.1242/dev.021170**.

16 B. Yao, *et al.*, Biochemical and structural cues of 3D-printed matrix synergistically direct MSC differentiation for functional sweat gland regeneration, *Sci. Adv.*, 2020, **6**(10), eaaz1094, DOI: **10.1126/sciadv.aaz1094**.

17 Y. Wang, *et al.*, TNF-α suppresses sweat gland differentiation of MSCs by reducing FTO-mediated m6A-demethylation of Nanog mRNA, *Sci. China: Life Sci.*, 2020, **63**(1), 80–91, DOI: **10.1007/s11427-019-9826-7**.

18 J. Cevik, *et al.*, The efficacy of three-dimensional printing for plastic surgery education: a narrative review, *Plast. Aesthet. Res.*, 2024, **11**, 39.

19 Y. Liu, *et al.*, Stiffness-mediated mesenchymal stem cell fate decision in 3D-bioprinted hydrogels, *Burns Trauma*, 2020, **8**, tkaa029, DOI: **10.1093/burnst/tkaa029**.

20 L. Ouyang, *et al.*, Three-dimensional bioprinting of embryonic stem cells directs highly uniform embryoid body formation, *Biofabrication*, 2015, **7**(4), 044101, DOI: **10.1088/1758-5090/7/4/04410**.

21 P. N. Bishop, The role of extracellular matrix in retinal vascular development and preretinal neovascularization, *Exp. Eye Res.*, 2015, **133**, 30–36, DOI: **10.1016/j.exer.2014.10.021**.

22 P. Akhyari, *et al.*, The quest for an optimized protocol for whole-heart decellularization: a comparison of three popular and a novel decellularization technique and their diverse effects on crucial extracellular matrix qualities, *Tissue Eng., Part C*, 2011, **17**(9), 915–926, DOI: **10.1089/ten.TEC.2011.0210**.

23 S. F. Badylak, *et al.*, Extracellular matrix as a biological scaffold material: Structure and function, *Acta Biomater.*, 2009, **5**(1), 1–13, DOI: **10.1016/j.actbio.2008.09.013**.

24 Y. Hong, *et al.*, Mechanical properties and in vivo behavior of a biodegradable synthetic polymer microfiber-extracellular matrix hydrogel biohybrid scaffold, *Biomaterials*, 2011, **32**(13), 3387–3394, DOI: **10.1016/j.biomaterials.2011.01.025**.

25 T. Jacob, *et al.*, Molecular and spatial landmarks of early mouse skin development, *Dev. Cell*, 2023, **58**(20), 2140–2162, DOI: **10.1016/j.devcel.2023.07.015**.

26 F. Shams, *et al.*, Overexpression of VEGF in dermal fibroblast cells accelerates the angiogenesis and wound healing function: in vitro and in vivo studies, *Sci. Rep.*, 2022, **12**(1), 18529, DOI: **10.1038/s41598-022-23304-8**.

27 X. Yuan, *et al.*, Reciprocal interaction between vascular niche and sweat gland promotes sweat gland regeneration, *Bioact. Mater.*, 2022, **21**, 340–357, DOI: **10.1016/j.bioactmat.2022.08.021**.

28 N. L. Heinecke, *et al.*, PepC: proteomics software for identifying differentially expressed proteins based on spectral counting, *Bioinformatics*, 2010, **26**(12), 1574–1575, DOI: **10.1093/bioinformatics/btq171**.

29 R. Palumbo, *et al.*, Extracellular HMGB1, a signal of tissue damage, induces mesoangioblast migration and prolifer-

ation, *J. Cell Biol.*, 2004, **164**(3), 441–449, DOI: **10.1083/jcb.200304135**.

30 D. Tang, *et al.*, The multifunctional protein HMGB1: 50 years of discovery, *Nat. Rev. Immunol.*, 2023, **23**(12), 824–841, DOI: **10.1038/s41577-023-00894-6**.

31 T. Starkova, *et al.*, Structure and Functions of HMGB2 Protein, *Int. J. Mol. Sci.*, 2023, **24**(9), 8334, DOI: **10.3390/ijms24098334**.

32 G. P. Sims, D. C. Rowe, S. T. Rietdijk, R. Herbst and A. J. Coyle, HMGB1 and RAGE in inflammation and cancer, *Annu. Rev. Immunol.*, 2010, **28**, 367–388.

33 F. Biscetti, G. Straface, R. De Cristofaro, S. Lancellotti, P. Rizzo, V. Arena, E. Stigliano, G. Pecorini, K. Egashira, G. De Angelis, G. Ghirlanda and A. Flex, High-mobility group box-1 protein promotes angiogenesis after peripheral

ischemia in diabetic mice through a VEGF-dependent mechanism, *Diabetes*, 2010, **59**, 1496–1505.

34 A. D. Dardenne, B. C. Wulff and T. A. Wilgus, The alarmin HMGB-1 influences healing outcomes in fetal skin wounds, *Wound Repair Regen.*, 2013, **21**, 282–291.

35 S. Straino, A. Di Carlo, A. Mangoni, R. De Mori, L. Guerra, R. Maurelli, L. Panacchia, F. Di Giacomo, R. Palumbo, C. Di Campli, L. Uccioli, P. Biglioli, M. E. Bianchi, M. C. Capogrossi and A. Germani, High-mobility group box 1 protein in human and murine skin: involvement in wound healing, *J. Invest. Dermatol.*, 2008, **128**, 1545–1553.

36 Q. Lin, X. P. Yang, D. Fang, X. Ren, H. Zhou, J. Fang, X. Liu, S. Zhou, F. Wen, X. Yao, J. M. Wang and S. B. Su, High-mobility group box-1 mediates Toll-like receptor 4-dependent angiogenesis, *Arterioscler. Thromb. Vasc. Biol.*, 2011, **31**, 1024–1032.